

Effects of Next-Nearest-Neighbor Repulsion on One-Dimensional Quarter-Filled Electron Systems

H. Yoshioka^{a*} M. Tsuchiizu^b and Y. Suzumura^{b,c}

^a*Department of Physics, Nara Women's University, Nara 630-8506*

^b*Department of Physics, Nagoya University, Nagoya 464-8602*

^c*CREST, Japan Science and Technology Corporation (JST)*

(Received September 12, 2000)

We examine effects of the next-nearest-neighbor repulsion on electronic states of a one-dimensional interacting electron system which consists of quarter-filled band and interactions of on-site and nearest-neighbor repulsion. We derive the effective Hamiltonian for the electrons around wave number $\pm k_F$ (k_F : Fermi wave number) and apply the renormalization group method to the bosonized Hamiltonian. It is shown that the next-nearest-neighbor repulsion makes $4k_F$ -charge ordering unstable and suppresses the spin fluctuation. Further the excitation gaps and spin susceptibility are also evaluated.

KEYWORDS: organic compounds, charge density waves, spin density waves, quarter-filling, long-range Coulomb interaction, spin gap

§1. Introduction

Quasi-one-dimensional organic conductors, many of which are the 2:1 charge transfer salts, exhibit a variety of physical properties depending on temperature, pressure and so on.¹⁾ A one-dimensional (1-D) interacting electron system at quarter-filling is a basic model for understanding such exotic properties. The electronic states of these materials have been often theoretically investigated by use of the model with only the on-site interaction U (> 0). Such a model with the on-site repulsion has been used to explain spin density wave (SDW) states observed experimentally.

Recent experiments on these materials indicate a coexistence of SDW with charge density wave (CDW).^{2,3,4,5)} In $(\text{TMTSF})_2\text{PF}_6$, $2k_F$ -SDW state coexists with $2k_F$ - and $4k_F$ -CDW below the SDW transition temperature,²⁾ while the two kinds of CDW's disappear below 3-4 K.⁴⁾ The material $(\text{DI-DCNQI})_2\text{Ag}$ shows the magnetic order of $2k_F$ -SDW below 5.5 K.⁶⁾ However, the analysis of ^{13}C -NMR spectra³⁾ suggests the $4k_F$ -CDW ordering below 220 K, which is much higher than the transition temperature of the magnetic order. Such a $4k_F$ -CDW order has been also observed in

* E-mail : yoshioka@phys.nara-wu.ac.jp

X-ray study.⁵⁾ It is known that the coexistence of SDW and CDW observed experimentally cannot be explained by a model with only the on-site repulsion. Therefore, it is necessary to treat models with the long-range components of Coulomb interaction, which may take crucial roles for these coexistent states.

Effects of several long-range interactions have been theoretically studied especially for a 1-D quarter-filled interacting electron system, and the rich phase diagram has been found. Numerical diagonalization of the model with both U and the nearest-neighbor interaction, V_1 ,^{7,8,9,10)} shows that the insulating phase appears for large strengths of both U and V_1 , and that the superconducting state becomes the most dominant fluctuation for large V_1 and small U . The mean-field theories have predicted the some coexistent states of SDW and CDW.^{11,12,13,14)} For the system with U and V_1 , a transition occurs from a pure $2k_F$ -SDW state to a coexistent state of $2k_F$ -SDW and $4k_F$ -CDW with increasing V_1 .¹¹⁾ It is maintained that such a coexistent state gives rise to the charge ordering in (DI-DCNQI)₂Ag.³⁾ The transition has been examined by evaluating the commensurability energy corresponding to the $8k_F$ -Umklapp scattering.¹²⁾ Kobayashi *et al.* found that the next-nearest-neighbor repulsion, V_2 , results in a coexistence of $2k_F$ -SDW and purely electronic $2k_F$ -CDW.¹³⁾ The problem has been reexamined by Tomio and one of the present authors¹⁴⁾ and it has been found that the coexistent state of $2k_F$ -SDW and $2k_F$ -CDW is followed by $4k_F$ -SDW but without $4k_F$ -CDW. The next-nearest-neighbor repulsion is the most promising candidate for the origin of the coexistence observed in (TMTSF)₂PF₆.^{2,4)}

In the previous works, we have analytically derived the $8k_F$ -Umklapp scattering for the electron system at quarter-filling with U and V_1 , and investigated the electronic properties by applying renormalization group (RG) method to the bosonized model.^{15,16)} The phase diagram has been determined on the plane of U and V_1 , which is qualitatively the same as that derived by the numerical approach. We found that the insulating state for both large U and V_1 exhibits the order of $4k_F$ -CDW with the most dominant fluctuation given by $2k_F$ -SDW. Such a state is similar to the coexistent state predicted by the mean-field theory and seems to correspond to the experimental observation in (DI-DCNQI)₂Ag that the characteristic temperature of the charge ordering is much larger than that of $2k_F$ -SDW.

In the present paper, we extend the previous method^{15,16)} to the system with U , V_1 and V_2 , and clarify the role of V_2 for the electronic states and the excitations.¹⁷⁾ We find that V_2 makes $4k_F$ -CDW state unstable and suppresses the spin fluctuation. The phase diagram is determined and compared with that by the mean-field theory. Electronic states are further examined by evaluating the excitation gaps of the charge and spin fluctuation, and spin susceptibility.

The plan of the paper is as follows. In §2, the effective Hamiltonian is derived and expressed in terms of bosonization with the phase variables. The phase diagram and excitations are determined by utilizing RG method in §3. Based on the RG equations, the spin susceptibility is calculated in

§4. Section 5 is devoted to summary.

§2. Model and Formulation

2.1 Effective Hamiltonian

We consider a 1-D electron system at quarter-filling. The Hamiltonian is given by $\mathcal{H} = \mathcal{H}_0 + \mathcal{H}_{\text{int}}$, where

$$\begin{aligned}\mathcal{H}_0 &= -t \sum_{j\sigma} \left(a_{j,\sigma}^\dagger a_{j+1,\sigma} + \text{h.c.} \right) - \mu \sum_{j,\sigma} n_{j,\sigma} \\ &= \sum_{K\sigma} (\epsilon_K - \mu) a_{K,\sigma}^\dagger a_{K,\sigma},\end{aligned}\tag{1}$$

$$\begin{aligned}\mathcal{H}_{\text{int}} &= \sum_{j\sigma\sigma'} \left\{ \frac{U}{2} \delta_{\sigma',-\sigma} n_{j,\sigma} n_{j,\sigma'} + V_1 n_{j,\sigma} n_{j+1,\sigma'} + V_2 n_{j,\sigma} n_{j+2,\sigma'} \right\} \\ &= \frac{1}{N_L} \sum_{\sigma\sigma'} \sum_{K_1 \sim K_4} \left\{ \frac{U}{2} \delta_{\sigma',-\sigma'} + V_1 e^{-i(K_2-K_3)a} + V_2 e^{-i2(K_2-K_3)a} \right\} \\ &\quad \times \delta_{K_1+K_2-K_3-K_4,G} a_{K_1,\sigma}^\dagger a_{K_2,\sigma'}^\dagger a_{K_3,\sigma'} a_{K_4,\sigma}.\end{aligned}\tag{2}$$

Here t and μ denote a transfer energy between the nearest-neighbor sites and a chemical potential, respectively, $\epsilon_K = -2t \cos Ka$ with a lattice constant a , and $-\pi/a < K \leq \pi/a$. The quantity $a_{j,\sigma}^\dagger (= 1/\sqrt{N_L} \sum_K e^{-iKaj} a_{K,\sigma}^\dagger)$ is a creation operator of the electron at the j -th site with spin $\sigma (= \pm)$, $n_{j,\sigma} = a_{j,\sigma}^\dagger a_{j,\sigma}$, $G = 0$ and $\pm 2\pi/a$, and N_L is the number of the lattice.

In order to obtain the effective Hamiltonian for the states near $\pm k_F$ ($k_F = \pi/(4a)$), the one-particle states are divided as shown in Fig. 1, *i.e.*, $d_{k,-,\sigma} = a_{K,\sigma}$ for $-\pi/a < K \leq -\pi/(2a)$, $c_{k,-,\sigma} = a_{K,\sigma}$ for $-\pi/(2a) < K \leq 0$, $c_{k,+,\sigma} = a_{K,\sigma}$ for $0 < K \leq \pi/(2a)$, and $d_{k,+,\sigma} = a_{K,\sigma}$ for $\pi/(2a) < K \leq \pi/a$, where k is deviation of the wave number from $\pm k_F$ for $c_{k,\pm,\sigma}$, and $\pm 3k_F$ for $d_{k,\pm,\sigma}$. Hereafter the one-particle states expressed by $d_{k,\pm,\sigma}$ ($c_{k,\pm,\sigma}$) are called as the upper (lower) band. In terms of $c_{k,p,\sigma}$ and $d_{k,p,\sigma}$ ($p = \pm$), \mathcal{H} is written as $\mathcal{H} = \mathcal{H}_0 + \sum_{i=0}^4 \mathcal{H}_{\text{int},i}$, where

$$\mathcal{H}_0 = \sum_{pk\sigma} \left\{ (\epsilon_{pk_F+k} - \mu) c_{k,p,\sigma}^\dagger c_{k,p,\sigma} + (\epsilon_{3pk_F+k} - \mu) d_{k,p,\sigma}^\dagger d_{k,p,\sigma} \right\},\tag{3}$$

$$\begin{aligned}\mathcal{H}_{\text{int},0} &= \frac{1}{L} \sum_{k,k',q} \sum_p \sum_{\sigma,\sigma'} \left(\frac{Ua}{2} \delta_{\sigma',-\sigma} - V_2 a \right) c_{k+q,p,\sigma}^\dagger c_{k'-q,-p,\sigma'}^\dagger c_{k',p,\sigma'} c_{k,-p,\sigma} \\ &\quad + \frac{1}{L} \sum_{k,k',q} \sum_p \sum_{\sigma,\sigma'} \left(\frac{Ua}{2} \delta_{\sigma',-\sigma} + V_1 a + V_2 a \right) c_{k+q,p,\sigma}^\dagger c_{k'-q,-p,\sigma'}^\dagger c_{k',-p,\sigma'} c_{k,p,\sigma} \\ &\quad + \frac{1}{L} \sum_{k,k',q} \sum_p \sum_{\sigma,\sigma'} \left(\frac{Ua}{2} \delta_{\sigma',-\sigma} + V_1 a + V_2 a \right) c_{k+q,p,\sigma}^\dagger c_{k'-q,p,\sigma'}^\dagger c_{k',p,\sigma'} c_{k,p,\sigma},\end{aligned}\tag{4}$$

$$\begin{aligned}\mathcal{H}_{\text{int},1} &= \frac{1}{L} \sum_{k,k',q} \sum_p \sum_{\sigma,\sigma'} (Ua \delta_{\sigma',-\sigma} - 2V_2 a) d_{k+q,p,\sigma}^\dagger c_{k'-q,-p,\sigma'}^\dagger c_{k',p,\sigma'} c_{k,p,\sigma} \\ &\quad + \frac{1}{L} \sum_{k,k',q} \sum_p \sum_{\sigma,\sigma'} (Ua \delta_{\sigma',-\sigma} - 2V_2 a) c_{k+q,p,\sigma}^\dagger c_{k'-q,p,\sigma'}^\dagger c_{k',-p,\sigma'} d_{k,p,\sigma},\end{aligned}\tag{5}$$

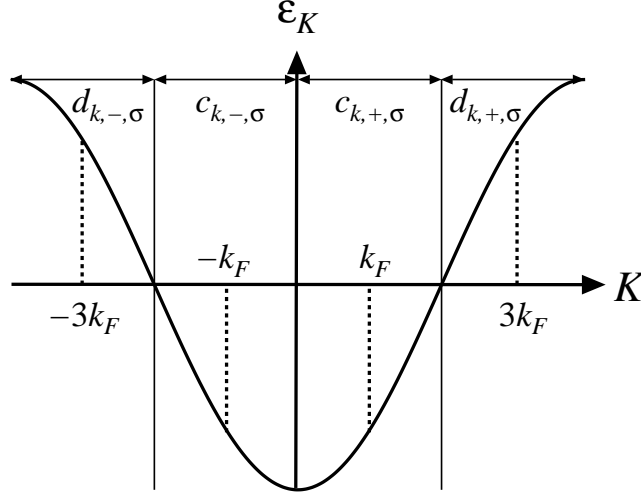


Fig. 1. The energy dispersion, $\epsilon_K = -2t \cos Ka$, in the present system.

$$\begin{aligned}
\mathcal{H}_{\text{int},2} = & \frac{1}{L} \sum_{k,k',q} \sum_p \sum_{\sigma,\sigma'} (Ua\delta_{\sigma',-\sigma} - 2V_2a) c_{k+q,p,\sigma}^\dagger d_{k'-q,p,\sigma'}^\dagger c_{k',p,\sigma'} d_{k,p,\sigma} \\
& + \frac{1}{L} \sum_{k,k',q} \sum_p \sum_{\sigma,\sigma'} (Ua\delta_{\sigma',-\sigma} + 2V_1a + 2V_2a) c_{k+q,p,\sigma}^\dagger d_{k'-q,p,\sigma'}^\dagger d_{k',p,\sigma'} c_{k,p,\sigma} \\
& + \frac{1}{L} \sum_{k,k',q} \sum_p \sum_{\sigma,\sigma'} \left(\frac{Ua}{2} \delta_{\sigma',-\sigma} - V_2a \right) \left\{ c_{k+q,p,\sigma}^\dagger c_{k'-q,-p,\sigma'}^\dagger d_{k',-p,\sigma'} d_{k,p,\sigma} + h.c. \right\} \\
& + \frac{1}{L} \sum_{k,k',q} \sum_p \sum_{\sigma,\sigma'} (Ua\delta_{\sigma',-\sigma} + 2V_1a + 2V_2a) c_{k+q,p,\sigma}^\dagger d_{k'-q,-p,\sigma'}^\dagger d_{k',-p,\sigma'} c_{k,p,\sigma} \\
& + \frac{1}{L} \sum_{k,k',q} \sum_p \sum_{\sigma,\sigma'} \left(\frac{Ua}{2} \delta_{\sigma',-\sigma} - V_1a + V_2a \right) \left\{ c_{k+q,p,\sigma}^\dagger c_{k'-q,-p,\sigma'}^\dagger d_{k',p,\sigma'} d_{k,-p,\sigma} + h.c. \right\} \\
& + \frac{1}{L} \sum_{k,k',q} \sum_p \sum_{\sigma,\sigma'} (Ua\delta_{\sigma',-\sigma} - 2V_1a + 2V_2a) c_{k+q,p,\sigma}^\dagger d_{k'-q,-p,\sigma'}^\dagger c_{k',p,\sigma'} d_{k,-p,\sigma} \\
& + \frac{1}{L} \sum_{k,k',q} \sum_p \sum_{\sigma,\sigma'} \left(\frac{Ua}{2} \delta_{\sigma',-\sigma} - V_1a + V_2a \right) \left\{ c_{k+q,p,\sigma}^\dagger c_{k'-q,p,\sigma'}^\dagger d_{k',-p,\sigma'} d_{k,-p,\sigma} + h.c. \right\} \\
& + \frac{1}{L} \sum_{k,k',q} \sum_p \sum_{\sigma,\sigma'} (Ua\delta_{\sigma',-\sigma} - 2V_1a + 2V_2a) c_{k+q,p,\sigma}^\dagger d_{k'-q,p,\sigma'}^\dagger c_{k',-p,\sigma'} d_{k,-p,\sigma} \\
& + \frac{1}{L} \sum_{k,k',q} \sum_p \sum_{\sigma,\sigma'} (Ua\delta_{\sigma',-\sigma} - 2V_2a) c_{k+q,p,\sigma}^\dagger d_{k'-q,p,\sigma'}^\dagger d_{k',-p,\sigma'} c_{k,-p,\sigma}, \tag{6}
\end{aligned}$$

$$\begin{aligned}
\mathcal{H}_{\text{int},3} = & \frac{1}{L} \sum_{k,k',q} \sum_p \sum_{\sigma,\sigma'} (Ua\delta_{\sigma',-\sigma} - 2V_2a) c_{k+q,p,\sigma}^\dagger d_{k'-q,-p,\sigma'}^\dagger d_{k',p,\sigma'} d_{k,p,\sigma} \\
& + \frac{1}{L} \sum_{k,k',q} \sum_p \sum_{\sigma,\sigma'} (Ua\delta_{\sigma',-\sigma} - 2V_2a) d_{k+q,p,\sigma}^\dagger d_{k'-q,p,\sigma'}^\dagger d_{k',-p,\sigma'} c_{k,p,\sigma}, \tag{7}
\end{aligned}$$

$$\begin{aligned}
\mathcal{H}_{\text{int},4} = & \frac{1}{L} \sum_{k,k',q} \sum_p \sum_{\sigma,\sigma'} \left(\frac{Ua}{2} \delta_{\sigma',-\sigma} - V_2a \right) d_{k+q,p,\sigma}^\dagger d_{k'-q,-p,\sigma'}^\dagger d_{k',p,\sigma'} d_{k,-p,\sigma} \\
& + \frac{1}{L} \sum_{k,k',q} \sum_p \sum_{\sigma,\sigma'} \left(\frac{Ua}{2} \delta_{\sigma',-\sigma} + V_1a + V_2a \right) d_{k+q,p,\sigma}^\dagger d_{k'-q,-p,\sigma'}^\dagger d_{k',-p,\sigma'} d_{k,p,\sigma} \\
& + \frac{1}{L} \sum_{k,k',q} \sum_p \sum_{\sigma,\sigma'} \left(\frac{Ua}{2} \delta_{\sigma',-\sigma} + V_1a + V_2a \right) d_{k+q,p,\sigma}^\dagger d_{k'-q,p,\sigma'}^\dagger d_{k',p,\sigma'} d_{k,p,\sigma}. \tag{8}
\end{aligned}$$

In the above expressions, $L = N_L a$ and the matrix elements of the interaction are calculated at $K = \pm k_F$ for the lower band and at $K = \pm 3k_F$ for the upper band. The elements, $(Ua/2\delta_{\sigma',-\sigma} + V_1a + V_2a)$, $(Ua/2\delta_{\sigma',-\sigma} - V_2a)$ and $(Ua/2\delta_{\sigma',-\sigma} - V_1a + V_2a)$ are originated from the interaction processes with the momentum transfer, 0 , $\pi/(2a)$ and π/a , respectively. Since there is no Umklapp scattering for only the lower band, *i.e.*, the first term of \mathcal{H}_0 and $\mathcal{H}_{\text{int},0}$, it is crucial to take account of the effects of the upper band in order to describe the insulating state of the quarter-filled 1-D electron systems.

By averaging the contribution from the upper band, the effective Hamiltonian describing the states near $\pm k_F$ is derived as follows. Representing $c_{k,p,\sigma}$ and $d_{k,p,\sigma}$ in terms of Grassmann variables, the partition function corresponding to eqs. (3)-(8) is written by $Z = \int \mathcal{D}[d_{k,p,\sigma}^* d_{k,p,\sigma}] \mathcal{D}[c_{k,p,\sigma}^* c_{k,p,\sigma}] e^{-S}$, where

$$S = S_{0c} + S_{0d} + \sum_{i=0}^4 S_{\text{int},i}, \tag{9}$$

$$S_{0c} = \sum_{p,k,\sigma} \int_0^\beta d\tau c_{k,p,\sigma}^* (\partial_\tau - \mu + \epsilon_{pk_F+k}) c_{k,p,\sigma}, \tag{10}$$

$$S_{0d} = \sum_{p,k,\sigma} \int_0^\beta d\tau d_{k,p,\sigma}^* (\partial_\tau - \mu + \epsilon_{3pk_F+k}) d_{k,p,\sigma}, \tag{11}$$

$$S_{\text{int},i} = \int_0^\beta d\tau \mathcal{H}_{\text{int},i}, \tag{12}$$

with $\beta = 1/T$ (T : temperature). After integrating with respect to $d_{k,p,\sigma}$, the partition function, Z , is given as $Z = Z_{0d} \int \mathcal{D}[c_{k,p,\sigma}^* c_{k,p,\sigma}] e^{-S_{\text{eff}}}$, where $Z_{0d} = \int \mathcal{D}[d_{k,p,\sigma}^* d_{k,p,\sigma}] e^{-S_{0d}}$, and $S_{\text{eff}} = S_{0c} - \ln \langle \exp(-\sum_{i=0}^4 S_{\text{int},i}) \rangle_d$ ($\langle A \rangle_d \equiv Z_{0d}^{-1} \int \mathcal{D}[d_{k,p,\sigma}^* d_{k,p,\sigma}] e^{-S_{0d}} A$). The perturbative expansion of S_{eff} leads to the effective Hamiltonian.

Up to the second order, the normal processes, $\mathcal{H}_{\text{int},n}$, which denote backward scattering and forward scattering, are derived as

$$\begin{aligned}
\mathcal{H}_{\text{int},n} = & \frac{1}{L} \sum_{k,k',q} \sum_p \sum_{\sigma,\sigma'} \left\{ (g_{1\perp} \delta_{\sigma-\sigma'} + g_{1\parallel} \delta_{\sigma\sigma'}) c_{k+q,p,\sigma}^\dagger c_{k'-q,-p,\sigma'}^\dagger c_{k',p,\sigma'} c_{k,-p,\sigma} \right. \\
& + (g_{2\perp} \delta_{\sigma-\sigma'} + g_{2\parallel} \delta_{\sigma\sigma'}) c_{k+q,p,\sigma}^\dagger c_{k'-q,-p,\sigma'}^\dagger c_{k',-p,\sigma'} c_{k,p,\sigma} \\
& \left. + (g_{4\perp} \delta_{\sigma-\sigma'} + g_{4\parallel} \delta_{\sigma\sigma'}) c_{k+q,p,\sigma}^\dagger c_{k'-q,p,\sigma'}^\dagger c_{k',p,\sigma'} c_{k,p,\sigma} \right\}. \tag{13}
\end{aligned}$$

The coupling constants are given as follows,

$$g_{1\parallel} = -V_2a - 4D_1(-V_2a)(-V_1a + V_2a), \quad (14)$$

$$g_{1\perp} = \frac{Ua}{2} - V_2a - 4D_1 \left(\frac{Ua}{2} - V_2a \right) \left(\frac{Ua}{2} - V_1a + V_2a \right), \quad (15)$$

$$g_{2\parallel} = V_1a + V_2a - 2D_1(-V_2a)^2 - 2D_1(-V_1a + V_2a)^2, \quad (16)$$

$$g_{2\perp} = \frac{Ua}{2} + V_1a + V_2a - 2D_1 \left(\frac{Ua}{2} - V_2a \right)^2 - 2D_1 \left(\frac{Ua}{2} - V_1a + V_2a \right)^2, \quad (17)$$

$$g_{4\parallel} = V_1a + V_2a - 2D_2(-V_1a + V_2a)^2, \quad (18)$$

$$g_{4\perp} = \frac{Ua}{2} + V_1a + V_2a - 2D_2 \left(\frac{Ua}{2} - V_1a + V_2a \right)^2, \quad (19)$$

where $D_1 = (8\pi ta)^{-1} \sqrt{2} \ln(\sqrt{2} + 1) \simeq 1.25/(8\pi ta)$ and $D_2 = (8\pi ta)^{-1} 2\sqrt{2}/(\sqrt{2} + 1) \sim 1.17/(8\pi ta)$. Note that eqs. (14)-(17) satisfy the condition, $g_{2\perp} - g_{2\parallel} + g_{1\parallel} = g_{1\perp}$, which corresponds to $SU(2)$ symmetry. The diagrams which lead to eqs. (14)-(19) are shown in Fig. 2, and the detailed calculation is given in Appendix A. The $8k_F$ -Umklapp scattering is obtained from the third order expansion shown in Fig. 3. The Hamiltonian for the Umklapp scattering is written as

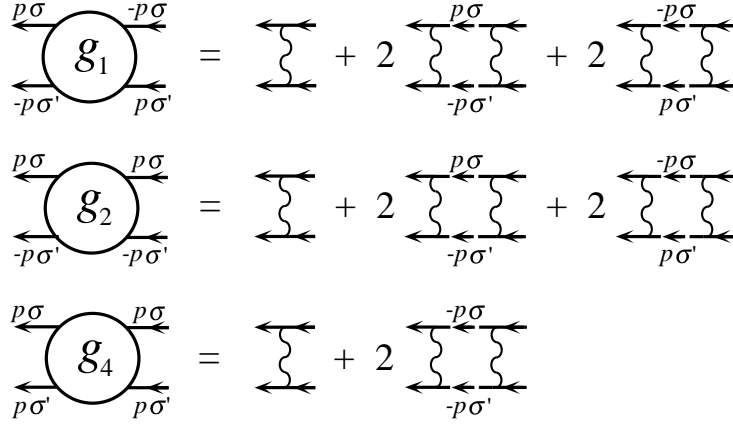


Fig. 2. Diagrams for the normal scattering. Here the dashed and wavy lines express the Green function of the upper bands and the interaction, respectively.

$$\mathcal{H}_{1/4} = g'_{1/4} \sum_p \int dx (\psi_{p,+}^\dagger \psi_{-p,+})^2 (\psi_{p,-}^\dagger \psi_{-p,-})^2, \quad (20a)$$

$$g'_{1/4} = \frac{1}{2t^2} \left\{ (Ua - 2V_2a)^2 (Ua - 4V_1a + V_2a) + 4(V_2a)^2 (Ua - 2V_1a + 2V_2a) \right\}, \quad (20b)$$

where $\psi_{p,\sigma} = 1/\sqrt{L} \sum_k e^{ikx} c_{k,p,\sigma}$. Detailed derivation of eqs. (20a) and (20b) is given in Appendix

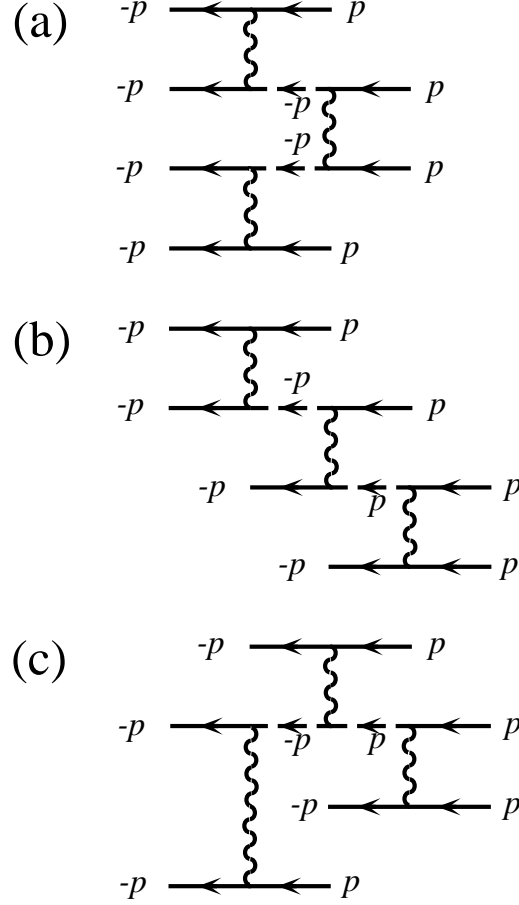


Fig. 3. Diagrams for the $8k_F$ -Umklapp scattering. The dashed and wavy lines express the Green function of the upper band and the interaction, respectively.

B. Thus, the effective Hamiltonian is written as

$$\mathcal{H}_{\text{eff}} = \mathcal{H}_{0c} + \mathcal{H}_{\text{int},n} + \mathcal{H}_{1/4}, \quad (21)$$

where $\mathcal{H}_{0c} = \sum_{pk\sigma} (\epsilon_{pk_F+k} - \mu) c_{k,p,\sigma}^\dagger c_{k,p,\sigma}$.

2.2 Bosonization

We linearize the energy dispersion as $\epsilon_{pk_F+k} - \mu \simeq pv_F k$ with $v_F = \sqrt{2}ta$ and utilize the bosonization method. The phase variables for the charge (spin) fluctuation, θ_ρ and ϕ_ρ , (θ_σ and ϕ_σ) are

defined as

$$\theta_{\rho(\sigma)} = \sum_{q \neq 0} \frac{\pi i}{qL} e^{-\alpha|q|/2 - iqx} \sum_{k,p} \left[c_{k+q,p,+}^\dagger c_{k,p,+} + (-) c_{k+q,p,-}^\dagger c_{k,p,-} \right], \quad (22)$$

$$\phi_{\rho(\sigma)} = \sum_{q \neq 0} \frac{\pi i}{qL} e^{-\alpha|q|/2 - iqx} \sum_{k,p} p \left[c_{k+q,p,+}^\dagger c_{k,p,+} + (-) c_{k+q,p,-}^\dagger c_{k,p,-} \right], \quad (23)$$

where α^{-1} is the ultraviolet cutoff. Those fields satisfy the commutation relations, $[\theta_\nu(x), \phi_{\nu'}(x')] = i\pi \operatorname{sgn}(x - x') \delta_{\nu\nu'}$ ($\nu, \nu' = \rho$ or σ). The electron operator is expressed as $\psi_{p,\sigma} = (2\pi\alpha)^{-1/2} \exp\{i(p/2)(\theta_\rho + p\phi_\rho + \sigma\theta_\sigma + \sigma p\phi_\sigma)\} \exp(i\pi\Xi_{p\sigma})$ with $\Xi_{p+} = p/2 \sum_{p'} \hat{N}_{p'+}$ and $\Xi_{p-} = p/2 \sum_{p'} \hat{N}_{p'-} + \sum_{p'} \hat{N}_{p'+}$ where $\hat{N}_{p\sigma} = \int dx \psi_{p\sigma}^\dagger \psi_{p\sigma}$. In terms of these phase variables, the effective Hamiltonian is expressed as $\mathcal{H}_{\text{eff}} = \mathcal{H}_\rho + \mathcal{H}_\sigma$, where

$$\mathcal{H}_\rho = \frac{v_\rho}{4\pi} \int dx \left\{ \frac{1}{K_\rho} (\partial_x \theta_\rho)^2 + K_\rho (\partial_x \phi_\rho)^2 \right\} + \frac{g_{1/4}}{2(\pi\alpha)^2} \int dx \cos 4\theta_\rho, \quad (24)$$

$$\mathcal{H}_\sigma = \frac{v_\sigma}{4\pi} \int dx \left\{ \frac{1}{K_\sigma} (\partial_x \theta_\sigma)^2 + K_\sigma (\partial_x \phi_\sigma)^2 \right\} + \frac{g_{1\perp}}{(\pi\alpha)^2} \int dx \cos 2\theta_\sigma. \quad (25)$$

Here $K_\nu = \sqrt{B_\nu/A_\nu}$ and $v_\nu = v_F \sqrt{B_\nu A_\nu}$ with $A_{\rho(\sigma)} = 1 + \{g_{4\parallel} + (-)g_{4\perp} + g_{2\parallel} + (-)g_{2\perp} - g_{1\parallel}\}/(\pi v_F)$ and $B_{\rho(\sigma)} = 1 + \{g_{4\parallel} + (-)g_{4\perp} - g_{2\parallel} - (+)g_{2\perp} + g_{1\parallel}\}/(\pi v_F)$. The coupling constant, $g_{1/4}$, is given by $g_{1/4} = g'_{1/4}/(2\pi\alpha)^2$. In terms of the phase variables, the order parameters for the $2k_F$ -SDW, $2k_F$ -CDW, $4k_F$ -CDW and $4k_F$ -bond order wave ($4k_F$ -BOW) are written as follows,

$$O_{2k_F\text{-SDW}} = \sum_{p\sigma} \sigma e^{-i2pk_F x} \psi_{p,\sigma}^\dagger \psi_{-p,\sigma} \propto \sin(2k_F x + \theta_\rho) \sin \theta_\sigma, \quad (26)$$

$$O_{2k_F\text{-CDW}} = \sum_{p\sigma} e^{-i2pk_F x} \psi_{p,\sigma}^\dagger \psi_{-p,\sigma} \propto \cos(2k_F x + \theta_\rho) \cos \theta_\sigma, \quad (27)$$

$$O_{4k_F\text{-CDW}} = \sum_p e^{-i4pk_F x} \psi_{p,+}^\dagger \psi_{p,-}^\dagger \psi_{-p,-} \psi_{-p,+} \propto \cos(4k_F x + 2\theta_\rho), \quad (28)$$

$$O_{4k_F\text{-BOW}} = \sum_p e^{-i4pk_F x} (ip) \psi_{p,+}^\dagger \psi_{p,-}^\dagger \psi_{-p,-} \psi_{-p,+} \propto \sin(4k_F x + 2\theta_\rho), \quad (29)$$

where the order parameter of $4k_F$ -BOW is given by the $4k_F$ -component of $n_{j,+} n_{j+1,-}$. Note that the third order perturbation for $\ln \langle \exp(-\sum_{i=0}^4 S_{\text{int},i}) \rangle_d$ shown in Fig. 3 generates the other $8k_F$ -Umklapp scattering term, $\cos 4\theta_\rho \cos 2\theta_\sigma$, which mixes the charge and spin fluctuation. Since the scaling dimension of this term is smaller than that of $\cos 4\theta_\rho$ or of $\cos 2\theta_\sigma$, we discard the term. The effects of the term are discussed in §5.

§3. Excitations and Phase Diagram

We investigate the excitations and the electronic states in the limit of low energy by using the RG method. At first, we consider the spin degree of freedom. By introducing $l = \ln(\alpha'/\alpha)$ as the new length scale $\alpha' (> \alpha)$, the RG equations for \mathcal{H}_σ are given as follows,¹⁸⁾

$$\frac{d}{dl} K_\sigma(l) = -\frac{1}{2} G_{1\perp}^2(l) K_\sigma^2(l), \quad (30)$$

$$\frac{d}{dl} G_{1\perp}(l) = [2 - 2K_\sigma(l)] G_{1\perp}(l), \quad (31)$$

where the initial conditions are given by $K_\sigma(0) = K_\sigma$ and $G_{1\perp}(0) = 2g_{1\perp}/\pi v_\sigma$. The behaviors of $K_\sigma(l)$ and $G_{1\perp}(l)$ are as follows. When $g_{1\perp} \geq 0$ (i.e., $U/2 \geq V_2$), the quantities, $G_{1\perp}(l)$ and $K_\sigma(l)$ tend to 0 and 1, respectively, and the excitation becomes gapless. Then the long-range correlation functions are given as $\langle \sin \theta_\sigma(x) \sin \theta_\sigma(0) \rangle \sim x^{-1} \ln^{1/2}(x)$ and $\langle \cos \theta_\sigma(x) \cos \theta_\sigma(0) \rangle \sim x^{-1} \ln^{-3/2}(x)$.¹⁹⁾ For $U/2 < V_2$, the spin gap appears due to $G_{1\perp}(l) \rightarrow -\infty$ and $K_\sigma(l) \rightarrow 0$. In this case, the phase, θ_σ , is locked as $0 \bmod \pi$ at the low energy limit and then $\langle \sin \theta_\sigma(x) \sin \theta_\sigma(0) \rangle$ vanishes exponentially and $\langle \cos \theta_\sigma(x) \cos \theta_\sigma(0) \rangle$ remains finite at the long distance. Therefore $2k_F$ -SDW does not exist. Thus it is found that the spin fluctuation is suppressed by V_2 .

Next we investigate the charge degree of freedom. The RG equations corresponding to \mathcal{H}_ρ are written as¹⁵⁾

$$\frac{d}{dl} K_\rho(l) = -8G_{1/4}^2(l)K_\rho^2(l), \quad (32)$$

$$\frac{d}{dl} G_{1/4}(l) = [2 - 8K_\rho(l)] G_{1/4}(l), \quad (33)$$

with the initial conditions given by $K_\rho(0) = K_\rho$ and $G_{1/4}(0) = g_{1/4}/(2\pi v_\rho)$. Correlation functions are calculated from the solutions of eqs. (32) and (33) as, $\langle \sin \theta_\rho(x) \sin \theta_\rho(0) \rangle = \langle \cos \theta_\rho(x) \cos \theta_\rho(0) \rangle \propto \exp\{-\int_0^{\ln x/\alpha} dl K_\rho(l)\}$, $\langle \cos 2\theta_\rho(x) \cos 2\theta_\rho(0) \rangle \propto \exp\{-\int_0^{\ln x/\alpha} dl [4K_\rho(l) + 2G_{1/4}(l)]\}$ and $\langle \sin 2\theta_\rho(x) \sin 2\theta_\rho(0) \rangle \propto \exp\{-\int_0^{\ln x/\alpha} dl [4K_\rho(l) - 2G_{1/4}(l)]\}$.²⁰⁾ Equations (32) and (33) are calculated analytically as¹⁶⁾

$$G_{1/4}^2(l) - 1/(2K_\rho(l)) - 2 \ln K_\rho(l) = A, \quad (34)$$

where A is a numerical constant determined by the initial conditions. Equation (34) is obtained by rewriting eq. (32) as $G_{1/4}^2(l) = (1/8)dK_\rho^{-1}(l)/dl$ and $K_\rho(l)G_{1/4}^2(l) = -(1/8)d \ln K_\rho(l)/dl$, which are substituted into eq. (33). By choosing some parameters, we show eq. (34) on the plane of K_ρ and $G_{1/4}$ in Fig. 4. In the region (a), the non-linear $G_{1/4}$ term becomes irrelevant leading to metallic state. Here the correlation functions with long distance are given by $\langle \sin \theta_\rho(x) \sin \theta_\rho(0) \rangle = \langle \cos \theta_\rho(x) \cos \theta_\rho(0) \rangle \sim x^{-K_\rho(\infty)}$ and $\langle \cos 2\theta_\rho(x) \cos 2\theta_\rho(0) \rangle \sim \langle \sin 2\theta_\rho(x) \sin 2\theta_\rho(0) \rangle \sim x^{-4K_\rho(\infty)}$. In particular, the initial values located between the thick solid curve and the thick dotted one are renormalized to $1/4 < K_\rho(\infty) < 1/3$ and $G_{1/4}(\infty) = 0$. Both regions (b) and (c) corresponds to the strong coupling regime with insulating states, in which $|G_{1/4}(l)| \rightarrow \infty$ and $K_\rho(l) \rightarrow 0$. In the region (b) where $G_{1/4}(l) \rightarrow -\infty$, the correlation functions, $\langle \cos 2\theta_\rho(x) \cos 2\theta_\rho(0) \rangle$, $\langle \cos \theta_\rho(x) \cos \theta_\rho(0) \rangle$, and $\langle \sin \theta_\rho(x) \sin \theta_\rho(0) \rangle$ remain finite at the long distance, whereas $\langle \sin 2\theta_\rho(x) \sin 2\theta_\rho(0) \rangle$ decays exponentially. Then both $2k_F$ -density waves and $4k_F$ -CDW states are stabilized. On the other hand, in the region (c) where $G_{1/4}(l) \rightarrow \infty$, one finds the finite value of $\langle \sin 2\theta_\rho(x) \sin 2\theta_\rho(0) \rangle$, $\langle \cos \theta_\rho(x) \cos \theta_\rho(0) \rangle$ and $\langle \sin \theta_\rho(x) \sin \theta_\rho(0) \rangle$ but the exponential decay for $\langle \cos 2\theta_\rho(x) \cos 2\theta_\rho(0) \rangle$. Therefore $4k_F$ -BOW and $2k_F$ -density waves are stabilized and $4k_F$ -CDW is completely suppressed. In Fig. 4, the closed circles, open circles and closed squares denote the initial values for $V_1/t = 1$,

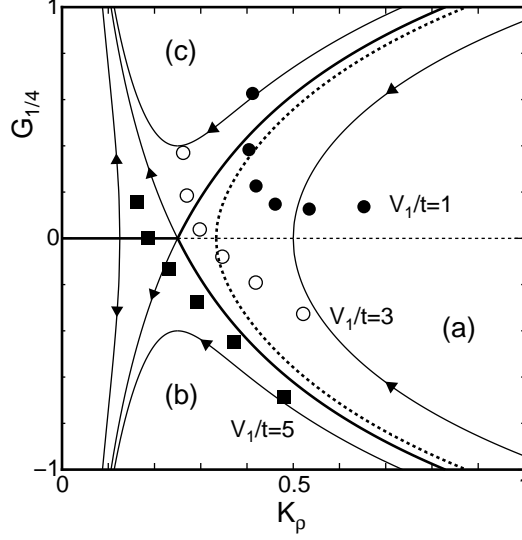


Fig. 4. Scaling flows of eq. (34) on the plane of K_ρ and $G_{1/4}$.^{16,17)} The thick solid curves denote the boundaries for metallic regions (a) and insulating regions (b) and (c). The fixed point for the thick dotted curve is given by $(K_\rho, G_{1/4}) = (1/3, 0)$. The closed circles, open circles and closed squares denote the initial values of $V_1/t = 1, 3$ and 5 , respectively, with the fixed $U/t = 6$, where respective points from right to left are $V_2/t = 0, 0.6, 1.2, 1.8, 2.4$ and 3.0 .

3 and 5, respectively, with the fixed $U/t = 6$, where respective points from right to left are $V_2/t = 0, 0.6, 1.2, 1.8, 2.4$ and 3.0 . Here $\alpha \simeq 2a/\pi$ is used.¹⁶⁾ Since increase of V_2 with fixed U and V_1 moves $(K_\rho, G_{1/4})$ to the region (c), it is found that the next-nearest-neighbor repulsion V_2 stabilizes $4k_F$ -BOW states.

By combining above consideration on the charge and spin degrees of freedom, we obtain the phase diagram, which is shown on the plane of V_1/t and V_2/t with fixed $U/t = 6$ in Fig. 5. Here the most dominant state of the respective region is as follows; $2k_F$ -SDW metal (I), $4k_F$ -CDW metal (IIa), $4k_F$ -BOW metal (IIb), $4k_F$ -CDW insulator (III), $4k_F$ -BOW insulator (IV), and $2k_F$ -CDW + $4k_F$ -BOW insulator (V). The region (I) with small V_1/t and V_2/t , which exhibits the gapless excitation for both charge and spin, denotes the metallic state with $2k_F$ -SDW as the most dominant fluctuation. In the region (III), the insulating ordered state of $4k_F$ -CDW appears, where $2k_F$ -SDW exists as the most dominant fluctuation. This comes from the fact that the parameters located in the metallic region (a) in Fig. 4 move to the insulating region (b) with increase of V_1 and fixed small V_2 , whereas the spin excitation remains gapless. Note that between the insulating state of $4k_F$ -CDW and the metallic state of $2k_F$ -SDW, the metallic state with the most dominant fluctuation of $4k_F$ -CDW exists (region (IIa)). Such a region is obtained for $1/4 < K_\rho(\infty) < 1/3$ and $g_{1/4} < 0$ (see Fig. 4). With increasing V_2/t , the parameters move from the region (b) to the region (c) in Fig. 4.

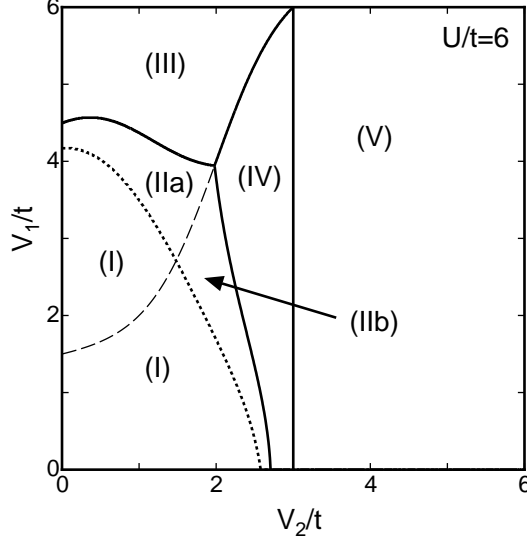


Fig. 5. The phase diagram on the plane of V_1/t and V_2/t at $U/t = 6$ where the thin dashed curve expresses $g_{1/4} = 0$. The states of respective regions are given by $2k_F$ -SDW metal (I), $4k_F$ -CDW metal (IIa), $4k_F$ -BOW metal (IIb), $4k_F$ -CDW insulator (III), $4k_F$ -BOW insulator (IV), and $2k_F$ -CDW + $4k_F$ -BOW insulator (V). In the region (III) and (IV), $2k_F$ -SDW exists as the dominant fluctuation.

In this case, the $4k_F$ -CDW state disappears and the ordered state of $4k_F$ -BOW appears (region (IV)), where the $2k_F$ -SDW state remains as the most dominant fluctuation as long as the spin excitation is gapless. The metallic state of $2k_F$ -SDW in the region (I) turns into the insulating $4k_F$ -BOW state (region (IV)) when V_2 increases with fixed small V_1 as seen from the closed circles with $V_1/t = 1$ in Fig. 4. With increasing V_2 further, the spin gap appears for $U < 2V_2$ and the insulating $2k_F$ -CDW + $4k_F$ -BOW state is realized in the region (V) since the correlation functions of $2k_F$ -SDW and of $4k_F$ -CDW are exponentially decayed at the long distance. In contrast to the region (IIa), there exists the metallic $4k_F$ -BOW state (region (IIb)) corresponding to $1/4 < K_\rho(\infty) < 1/3$ and $g_{1/4} > 0$ between the region (I) and (IV).

Figure 6 shows the charge gap Δ_ρ (a) and the spin gap Δ_σ (b) as a function of V_2 with choices of $V_1/t = 6$, $V_1/t = 5$ and $V_1/t = 3.5$ for $U/t = 6$. By using the solution of the RG equations, (30)-(33), the quantities Δ_ρ and Δ_σ are determined by the following condition, $\Delta_\rho = v_\rho \alpha^{-1} \exp(-l_\rho)$ with $|G_{1/4}(l_\rho)| = 1$,¹⁵⁾ and $\Delta_\sigma = v_\sigma \alpha^{-1} \exp(-l_\sigma)$ with $G_{1\perp}(l_\sigma) = -2$. Note that the spin gap determined by such a method shows quantitatively good agreement with that obtained from the exact solution²²⁾ for $\Delta_\sigma/t < 1$ in case of negative U Hubbard model. For $V_1/t = 6$ and 5, the charge gap is finite except for the boundary between the region (III) and the region (IV) in Fig. 5. In the regions (IV) and (V), Δ_ρ increases monotonously with V_2 . In the region (III), Δ_ρ for $V_1/t = 5$

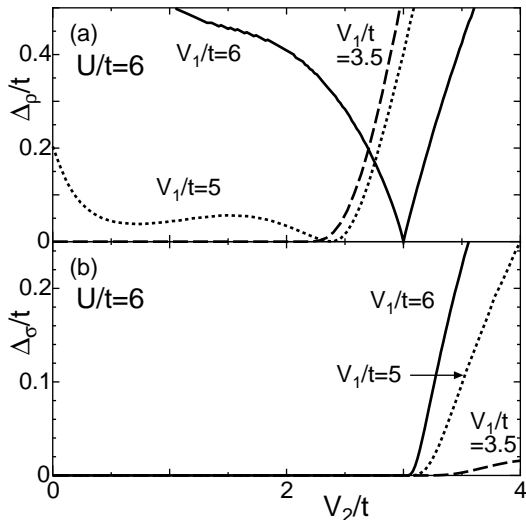


Fig. 6. The charge gap Δ_ρ (a) and the spin gap Δ_σ (b) as a function of V_2 at $U/t = 6$ with choices of $V_1/t = 6$ (solid curve), $V_1/t = 5$ (dotted curve) and $V_1/t = 3.5$ (dashed curve).

does not show a monotonous behavior as a function of V_2 , whereas Δ_ρ for $V_1/t = 6$ decreases with increase of V_2 . Such a behavior of Δ_ρ for $V_1/t = 5$ may come from the fact that the boundary between the region (IIa) and the region (III) is not a monotonous function of V_2 . As mentioned above, the condition for appearance of the spin gap is given by $U < 2V_2$ and then independent of V_1 . However, as seen in Fig. 6(b), the magnitude of the spin gap does depend on the value of V_1 , which enhances the spin gap.

Here we note the case of small U . The metallic state is realized for all regions corresponding to Fig. 5, *i.e.*, the region for $V_1 < U$ and $V_2 < U$. In this case, the new metallic state appears for $U < 2V_2$ in which the spin gap exists as shown in just below eq. (31). In this metallic state, the most dominant fluctuation is $2k_F$ -CDW for $K_\rho(\infty) < 1$.

Finally, we consider correspondence between the present state and the coexistent state found by the mean-field theory. As discussed in the previous paper,¹⁶⁾ the insulating $4k_F$ -CDW states in the region (III) corresponds to the coexistent state of $4k_F$ -CDW and $2k_F$ -SDW¹¹⁾ because the most dominant fluctuation of $2k_F$ -SDW exists in the region (III). In the insulating $4k_F$ -BOW state (IV), the fluctuations of both $2k_F$ -CDW and $2k_F$ -SDW develop, whereas the $4k_F$ -CDW state is completely suppressed. Therefore, the state of the region (IV) may correspond to the coexistent states of two kinds of $2k_F$ -density waves¹³⁾ without $4k_F$ -CDW.¹⁴⁾

§4. Spin Susceptibility

In this section, the spin susceptibility of the present system is investigated. We utilize the formula developed in ref. 21, which is effective at relatively low temperatures since it is based on the RG analysis using the linearized band. From eqs. (30) and (31), one obtains

$$g_{1\perp}(l) = \frac{g_{1\perp}}{1 + 2g_{1\perp}(\pi v_{\sigma}^0)^{-1}l}, \quad (35)$$

where $g_{1\perp}/(\pi v_{\sigma}^0) \ll 1$ and $v_{\sigma}^0 = v_F \left\{ 1 + (g_{4\parallel} - g_{4\perp})(\pi v_F)^{-1} \right\}$. By using eq. (35), the spin susceptibility, $\chi_{\sigma}(T)$, is calculated as²¹⁾

$$\chi_{\sigma}(T) = \frac{1}{2} \frac{\chi_p^0(T)}{1 - \{g_{4\perp} - g_{4\parallel} + g_{1\perp}(l)\}\chi_p^0(T)}, \quad (36)$$

$$\chi_p^0(T) = -\frac{2}{L} \sum_k \lim_{q \rightarrow 0} \frac{f(\epsilon_{pk_F+k}) - f(\epsilon_{pk_F+k+q})}{\epsilon_{pk_F+k} - \epsilon_{pk_F+k+q}}, \quad (37)$$

where $f(\epsilon) = 1/(e^{(\epsilon-\mu)/T} + 1)$ and $l = \ln(v_F \alpha^{-1}/T)$. In Fig. 7, $\chi_{\sigma}(T)/\chi^0(0)$ is shown where $\chi^0(0)$ denotes the susceptibility in the absence of the interaction at $T = 0$. At high temperatures,

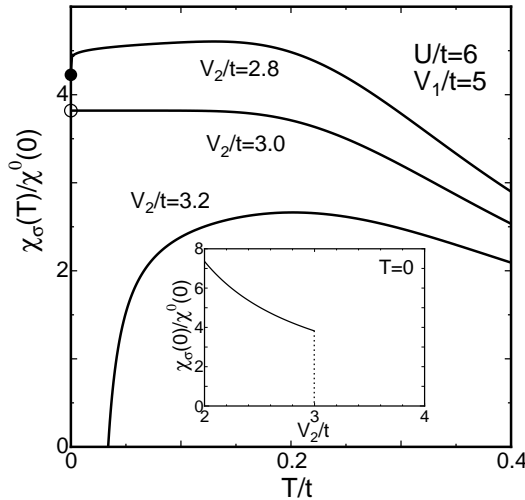


Fig. 7. Normalized spin susceptibility, $\chi_{\sigma}(T)/\chi^0(0)$, where $\chi^0(0)$ is the susceptibility in the absence of the interaction at $T = 0$, as a function of T/t for the several choice of V_2 with fixed $U/t = 6$ and $V_1/t = 5$. The black and white circles denote the values of $T = 0$ for $U > 2V_2$ and $U = 2V_2$, respectively. Inset : Spin susceptibility at $T = 0$ as a function of V_2/t with fixed $U/t = 6$ and $V_1/t = 5$.

the spin susceptibility increases with decreasing temperature. In the limit of zero temperature, the susceptibility approaches to a constant with infinite slope for $U > 2V_2$ as seen in Hubbard model.²¹⁾ Since it is due to logarithmic temperature dependence of $g_{1\perp}(l)$, such an anomaly is not

observed for $U = 2V_2$. In case of the strong coupling, *i.e.*, $U < 2V_2$, the susceptibility vanishes near the temperature, $T_{SG} = v_F \alpha^{-1} \exp\{\pi v_\sigma^0 / (2g_{1\perp})\}$, which originates from the fact that we use the solution of the weak coupling expansion, eq. (35). It is expected that the susceptibility for $T \ll T_{SG}$ behaves as $(\Delta_\sigma/T)^{1/2} \exp\{-\Delta_\sigma/T\}^{23}$ where Δ_σ is the spin gap. The inset shows $\chi_\sigma(0)/\chi^0(0)$ as a function of V_2/t with fixed $U/t = 6$ and $V_1/t = 5$. The interaction V_2 suppresses the spin fluctuation monotonously even for the region without the spin gap. On the other hand, V_1 enhances $\chi_\sigma(0)/\chi^0(0)$. These are due to the effect from the upper band because $\chi_\sigma(0)/\chi^0(0) = \left\{1 + (g_{4\parallel} - g_{4\perp})(\pi v_F)^{-1}\right\}^{-1}$ with $g_{4\parallel} - g_{4\perp} = -Ua/2\{1 - 2D_2(Ua/2 - 2V_1a + 2V_2a)\}$. Note that the spin susceptibility in case of $V_1 = V_2 = 0$ is different from that derived in ref. 21 because our formula includes the virtual process to the upper band. Spin susceptibilities both with and without the virtual processes are compared with that derived from the exact solution²⁴ in Appendix C.

§5. Summary

We investigated the electronic states and excitations of the one-dimensional electron system at quarter-filling with on-site (U), nearest-neighbor (V_1) and next-nearest-neighbor (V_2) repulsive interactions. By taking account of the effects of the upper band in a perturbative way, the effective Hamiltonian has been obtained in terms of the phase variables and analyzed by the renormalization group method.

The following roles of V_2 have been found. The spin fluctuation is suppressed with increasing V_2 and the spin gap is obtained for $V_2 > U/2$. Such a characteristic behavior can be seen in the spin susceptibility, $\chi_\sigma(T)$, where $\chi_\sigma(0)$ decreases with increasing V_2 and vanishes for $V_2 > U/2$. Note that the decrease of $\chi_\sigma(0)$ by V_2 for $U/2 > V_2$ is due to the effects of the upper band. In addition, the interaction suppresses the $4k_F$ -CDW state and stabilizes the $4k_F$ -BOW state. As a result, the insulating state of $4k_F$ -CDW realized for large U and V_1 changes into the insulating state of $4k_F$ -BOW with increasing V_2 . The insulating $4k_F$ -BOW state moves to the insulating states of $4k_F$ -BOW + $2k_F$ -CDW with increasing V_2 further. Thus the charge distribution changes from $(\bigcirc \circ \bigcirc \circ)$ of $4k_F$ -CDW to $(\bigcirc \bigcirc \circ \circ)$ of $2k_F$ -CDW with increase of V_2 where \bigcirc (\circ) denotes the rich (poor) charge at the respective site. The excitation gaps were determined as a function of V_2 with several choices of V_1 at $U/t = 6$ from the solutions of the RG equations. In the states of insulating $4k_F$ -BOW and $4k_F$ -BOW + $2k_F$ -CDW, the charge gap increases as a function of V_2 , whereas the gap is not a monotonous function of V_2 in the insulating $4k_F$ -CDW state when parameters are located near the boundary of metal insulator transition. The spin gap appears independently of the value of V_1 . However, the magnitude of the spin gap does depend on V_1 , which enhances the spin gap. For the case of weak on-site repulsion, the ground state for $V_1 < U$ is metallic. When V_2 is added to the state, the metallic state with spin gap appears, where the dominant fluctuation is given by the $2k_F$ -CDW.

In the present treatment, we have neglected the other $8k_F$ -Umklapp scattering term,

$\cos 4\theta_\rho \cos 2\theta_\sigma$, which mixes the charge and spin degrees of freedom and has the scaling dimension less than that of $\cos 2\theta_\sigma$ or of $\cos 4\theta_\rho$. The importance of such a term has been pointed out for half-filling extended Hubbard model with $U + V_1$,^{25,26,27} in which a term $\cos 2\theta_\rho \cos 2\theta_\sigma$ exists besides $\cos 2\theta_\rho$ and $\cos 2\theta_\sigma$ (the definitions of the phases and the interaction correspond to ours). In the half-filling model with $U + V_1$, the coefficient of $\cos 2\theta_\rho$ and of $\cos 2\theta_\sigma$ vanishes at $U = 2V_1$, whereas the term $\cos 2\theta_\rho \cos 2\theta_\sigma$ is finite. Thus the new phase appears near $U \simeq 2V_1$.²⁷ In the present model, the coefficient of $\cos 4\theta_\rho$ and that of $\cos 2\theta_\sigma$ become zero simultaneously at the point, $U = V_1 = 2V_2$. In this point, the coefficient of $\cos 4\theta_\rho \cos 2\theta_\sigma$ also vanishes (see Appendix B). Therefore, it is expected that such a term does not change the phase diagram qualitatively, but may result in only a quantitative change.

The appearance of the spin gap and the variation of the charge order with increasing V_2 are of interest and may be observed by the increase of the pressure along the conducting chain.²⁸

Acknowledgment

The authors would like to thank H. Fukuyama, T. Itakura, H. Seo, Y. Tomio for stimulating discussions. This work was partly supported by a Grant-in-Aid for Scientific Research from the Ministry of Education, Science, Sports and Culture, (No.11740196) and by a Grant-in-Aid for Scientific Research from the Ministry of Education, Science, Sports and Culture, (No.09640429).

Appendix A: Derivation of the normal processes

From Fig. 2, the matrix elements are given as

$$g_{1,\sigma\sigma'} = X_{2k_F,\sigma\sigma'} - 4\frac{1}{\beta L} \sum_{-\pi/(4a) < k \leq \pi/4a} \sum_{\epsilon_n} X_{2k_F,\sigma\sigma'} X_{4k_F,\sigma\sigma'} G_p(i\epsilon_n, k) G_{-p}(-i\epsilon_n, -k), \quad (\text{A}\cdot 1)$$

$$g_{2,\sigma\sigma'} = X_{0,\sigma\sigma'} - 2\frac{1}{\beta L} \sum_{-\pi/(4a) < k \leq \pi/4a} \sum_{\epsilon_n} \{X_{2k_F,\sigma\sigma'}^2 + X_{4k_F,\sigma\sigma'}^2\} G_p(i\epsilon_n, k) G_{-p}(-i\epsilon_n, -k), \quad (\text{A}\cdot 2)$$

$$g_{4,\sigma\sigma'} = X_{0,\sigma\sigma'} - 2\frac{1}{\beta L} \sum_{-\pi/(4a) < k \leq \pi/4a} \sum_{\epsilon_n} X_{4k_F,\sigma\sigma'}^2 G_p(i\epsilon_n, k) G_{-p}(-i\epsilon_n, -k), \quad (\text{A}\cdot 3)$$

where $g_{i,\sigma\sigma} = g_{i\parallel}$ and $g_{i,\sigma-\sigma} = g_{i\perp}$ ($i=1,2,4$). The quantities, $X_{0,\sigma\sigma'}$, $X_{2k_F,\sigma\sigma'}$ and $X_{4k_F,\sigma\sigma'}$ are the matrix elements of the interaction, $X_{0,\sigma\sigma'} = Ua/2\delta_{\sigma,-\sigma'} + V_1a + V_2a$, $X_{2k_F,\sigma\sigma'} = Ua/2\delta_{\sigma,-\sigma'} - V_2a$ and $X_{4k_F,\sigma\sigma'} = Ua/2\delta_{\sigma,-\sigma'} - V_1a + V_2a$, respectively. The green function of the upper band is given by $G_p(i\epsilon_n, k) = 1/(i\epsilon_n - \epsilon_{3pk_F+k} + \mu)$. The particle-particle propagators are calculated as,

$$\begin{aligned} D_1 &= \frac{1}{\beta L} \sum_{-\pi/(4a) < k \leq \pi/4a} \sum_{\epsilon_n} G_p(i\epsilon_n, k) G_{-p}(-i\epsilon_n, -k) \\ &= \frac{1}{L} \sum_{-\pi/(4a) < k \leq \pi/4a} \frac{1}{2(\epsilon_{3pk_F+k} - \mu)} \{1 - 2f(\epsilon_{3pk_F+k} - \mu)\} \\ &\simeq \frac{1}{8\pi ta} \int_0^{\pi/2} dy \frac{1}{\sin y + 1/\sqrt{2}} = \frac{\sqrt{2}}{8\pi ta} \ln(\sqrt{2} + 1), \end{aligned} \quad (\text{A}\cdot 4)$$

$$\begin{aligned}
D_2 &= \frac{1}{\beta L} \sum_{-\pi/(4a) < k \leq \pi/4a} \sum_{\epsilon_n} G_p(i\epsilon_n, k) G_p(-i\epsilon_n, -k) \\
&= \frac{1}{L} \sum_{-\pi/(4a) < k \leq \pi/4a} \frac{1}{\epsilon_{3pk_F+k} + \epsilon_{3pk_F-k} - 2\mu} \{1 - f(\epsilon_{3pk_F+k} - \mu) - f(\epsilon_{3pk_F-k} - \mu)\} \\
&\simeq \frac{1}{4\pi t a} \int_0^{\pi/2} dy \frac{1}{\sin y + \cos y + \sqrt{2}} = \frac{1}{8\pi t a} \frac{2\sqrt{2}}{\sqrt{2} + 1}, \tag{A.5}
\end{aligned}$$

where $f(\epsilon) = 1/(e^{\beta\epsilon} + 1)$. Here $f(\epsilon_{3pk_F \pm k} - \mu)$ is treated as zero because the energy scale we consider is smaller than $-\mu = \sqrt{2}t$. Equations (A.1)-(A.5) give rise to eqs. (14)-(19).

Appendix B: Derivation of Umklapp scattering

As shown in Fig. 3, the $8k_F$ -Umklapp scattering consists of the interaction processes, in which the right moving four electrons are scattered into the left moving states and vice versa. Such processes are derived from $\langle S_{\text{int},1}^2 S_{\text{int},2} \rangle_d / 2$ among the third order perturbation. The processes in Fig. 3(a), (b) and (c) are written as S_a , S_b and S_c , respectively, where

$$\begin{aligned}
S_a &= \frac{1}{2L^3} \sum_p \sum_{\sigma_1, \sigma'_1} \sum_{k_1, k'_1, q_1} \int_0^\beta d\tau_1 2X_{2k_F, \sigma_1 \sigma'_1} \sum_{\sigma_2, \sigma'_2} \sum_{k_2, k'_2, q_2} \int_0^\beta d\tau_2 2X_{2k_F, \sigma_2 \sigma'_2} \sum_{\sigma_3, \sigma'_3} \sum_{k_3, k'_3, q_3} \int_0^\beta d\tau_3 2X_{4k_F, \sigma_3 \sigma'_3} \\
&\times \left\{ \langle c_{k_1+q_1, -p, \sigma_1}^*(\tau_1) c_{k'_1-q_1, -p, \sigma'_1}^*(\tau_1) c_{k'_1, p, \sigma'_1}(\tau_1) d_{k_1, -p, \sigma_1}(\tau_1) \right. \\
&\times c_{k_2+q_2, -p, \sigma_2}^*(\tau_2) c_{k'_2-q_2, -p, \sigma'_2}^*(\tau_2) c_{k'_2, p, \sigma'_2}(\tau_2) d_{k_2, -p, \sigma_2}(\tau_2) \\
&\times \left. d_{k_3+q_3, -p, \sigma_3}^*(\tau_3) d_{k'_3-q_3, -p, \sigma'_3}^*(\tau_3) c_{k'_3, p, \sigma'_3}(\tau_3) c_{k_3, p, \sigma_3}(\tau_3) \rangle_d + h.c. \right\}, \tag{B.1}
\end{aligned}$$

$$\begin{aligned}
S_b &= \frac{1}{L^3} \sum_p \sum_{\sigma_1, \sigma'_1} \sum_{k_1, k'_1, q_1} \int_0^\beta d\tau_1 2X_{2k_F, \sigma_1 \sigma'_1} \sum_{\sigma_2, \sigma'_2} \sum_{k_2, k'_2, q_2} \int_0^\beta d\tau_2 2X_{2k_F, \sigma_2 \sigma'_2} \sum_{\sigma_3, \sigma'_3} \sum_{k_3, k'_3, q_3} \int_0^\beta d\tau_3 2X_{4k_F, \sigma_3 \sigma'_3} \\
&\times \langle d_{k_1+q_1, p, \sigma_1}^*(\tau_1) c_{k'_1-q_1, -p, \sigma'_1}^*(\tau_1) c_{k'_1, p, \sigma'_1}(\tau_1) c_{k_1, p, \sigma_1}(\tau_1) \\
&\times c_{k_2+q_2, -p, \sigma_2}^*(\tau_2) c_{k'_2-q_2, -p, \sigma'_2}^*(\tau_2) c_{k'_2, p, \sigma'_2}(\tau_2) d_{k_2, -p, \sigma_2}(\tau_2) \\
&\times c_{k_3+q_3, -p, \sigma_3}^*(\tau_3) d_{k'_3-q_3, -p, \sigma'_3}^*(\tau_3) c_{k'_3, p, \sigma'_3}(\tau_3) d_{k_3, p, \sigma_3}(\tau_3) \rangle_d, \tag{B.2}
\end{aligned}$$

$$\begin{aligned}
S_c &= \frac{1}{L^3} \sum_p \sum_{\sigma_1, \sigma'_1} \sum_{k_1, k'_1, q_1} \int_0^\beta d\tau_1 2X_{2k_F, \sigma_1 \sigma'_1} \sum_{\sigma_2, \sigma'_2} \sum_{k_2, k'_2, q_2} \int_0^\beta d\tau_2 2X_{2k_F, \sigma_2 \sigma'_2} \sum_{\sigma_3, \sigma'_3} \sum_{k_3, k'_3, q_3} \int_0^\beta d\tau_3 2X_{2k_F, \sigma_3 \sigma'_3} \\
&\times \langle d_{k_1+q_1, p, \sigma_1}^*(\tau_1) c_{k'_1-q_1, -p, \sigma'_1}^*(\tau_1) c_{k'_1, p, \sigma'_1}(\tau_1) c_{k_1, p, \sigma_1}(\tau_1) \\
&\times c_{k_2+q_2, -p, \sigma_2}^*(\tau_2) c_{k'_2-q_2, -p, \sigma'_2}^*(\tau_2) c_{k'_2, p, \sigma'_2}(\tau_2) d_{k_2, -p, \sigma_2}(\tau_2) \\
&\times c_{k_3+q_3, -p, \sigma_3}^*(\tau_3) d_{k'_3-q_3, -p, \sigma'_3}^*(\tau_3) d_{k'_3, p, \sigma'_3}(\tau_3) c_{k_3, p, \sigma_3}(\tau_3) \rangle_d. \tag{B.3}
\end{aligned}$$

In eq. (B.1), the average, $\langle \dots \rangle_d$ is calculated as,

$$\begin{aligned}
& - \langle d_{k_1, -p, \sigma_1}(\tau_1) d_{k_2, -p, \sigma_2}(\tau_2) d_{k_3+q_3, -p, \sigma_3}^*(\tau_3) d_{k'_3-q_3, -p, \sigma'_3}^*(\tau_3) \rangle_d \\
&= -G_{-p}(\tau_1 - \tau_3, k_1) G_{-p}(\tau_2 - \tau_3, k_2) \left(\delta_{k_3+q_3, k_2} \delta_{k'_3-q_3, k_1} \delta_{\sigma_3, \sigma_2} \delta_{\sigma'_3, \sigma_1} - \delta_{k_3+q_3, k_1} \delta_{k'_3-q_3, k_2} \delta_{\sigma_3, \sigma_1} \delta_{\sigma'_3, \sigma_2} \right) \\
&\simeq -\frac{1}{8t^2} \delta(\tau_1 - \tau_3) \delta(\tau_2 - \tau_3) \left(\delta_{k_3+q_3, k_2} \delta_{k'_3-q_3, k_1} \delta_{\sigma_3, \sigma_2} \delta_{\sigma'_3, \sigma_1} - \delta_{k_3+q_3, k_1} \delta_{k'_3-q_3, k_2} \delta_{\sigma_3, \sigma_1} \delta_{\sigma'_3, \sigma_2} \right). \tag{B.4}
\end{aligned}$$

Here the green function, $G_p(\tau, k) = \beta^{-1} \sum_{\epsilon_n} e^{-i\epsilon_n \tau} G_p(i\epsilon_n, k)$, is replaced by $-1/(2\sqrt{2}t)\delta(\tau)$. By substituting eq. (B·4) into eq. (B·1),

$$S_a = \frac{1}{8t^2} \sum_p \sum_{\sigma_1, \sigma'_1} \sum_{\sigma_2, \sigma'_2} 2X_{2k_F, \sigma_1 \sigma'_1} \times 2X_{2k_F, \sigma_2 \sigma'_2} \times 2X_{4k_F, \sigma_2 \sigma_1} \\ \times \frac{1}{L^3} \sum_{q_1, q_2, q_3} \int_0^\beta d\tau A_{p\sigma_1}(q_1 - q_3) A_{p\sigma_2}(q_2 + q_3) A_{p\sigma'_1}(-q_1) A_{p\sigma'_2}(-q_2), \quad (\text{B}\cdot 5)$$

where $A_{p, \sigma}(q) = \sum_k c_{k+q, p, \sigma}^* c_{k, -p, \sigma}$. In a similar calculation, one obtains $S_b = S_a$ and

$$S_c = \frac{1}{8t^2} \sum_p \sum_{\sigma_1, \sigma'_1} \sum_{\sigma'_2, \sigma_3} 2X_{2k_F, \sigma_1 \sigma'_1} \times 2X_{2k_F, \sigma_1 \sigma'_2} \times 2X_{2k_F, \sigma_3 \sigma_1} \\ \times \frac{1}{L^3} \sum_{q_1, q_2, q_3} \int_0^\beta d\tau A_{p\sigma_1}(q_1 - q_3) A_{p\sigma'_1}(q_2 + q_3) A_{p\sigma'_2}(-q_1) A_{p\sigma_3}(-q_2). \quad (\text{B}\cdot 6)$$

Here we introduce the field operator, $\psi_{p, \sigma} = 1/\sqrt{L} \sum_k e^{ikx} c_{k, p, \sigma}$ and write the Hamiltonian corresponding to the above action, $\mathcal{H}'_{1/4}$, as

$$\mathcal{H}'_{1/4} = \frac{1}{4t^2} \sum_p \sum_{\sigma_1, \sigma'_1} \sum_{\sigma_2, \sigma'_2} 2X_{2k_F, \sigma_1 \sigma'_1} \times 2X_{2k_F, \sigma_2 \sigma'_2} \times 2X_{4k_F, \sigma_2 \sigma_1} \int dx A_{p\sigma_1} A_{p\sigma_2} A_{p\sigma'_1} A_{p\sigma'_2} \\ + \frac{1}{8t^2} \sum_p \sum_{\sigma_1, \sigma'_1} \sum_{\sigma'_2, \sigma_3} 2X_{2k_F, \sigma_1 \sigma'_1} \times 2X_{2k_F, \sigma_1 \sigma'_2} \times 2X_{2k_F, \sigma_3 \sigma_1} \int dx A_{p\sigma_1} A_{p\sigma'_2} A_{p\sigma'_1} A_{p\sigma_3}, \quad (\text{B}\cdot 7)$$

where $A_{p, \sigma} = \psi_{p, \sigma}^\dagger \psi_{-p, \sigma}$. The above Hamiltonian can be rewritten as $\mathcal{H}'_{1/4} = \mathcal{H}_{1/4} + \mathcal{H}_{1/4}^a + \mathcal{H}_{1/4}^b$, where

$$\mathcal{H}_{1/4} = \frac{1}{4t^2} \sum_{p, \sigma} \left\{ (2X_{2k_F, \sigma-\sigma})^2 (2X_{4k_F, \sigma\sigma} + 2X_{4k_F, \sigma-\sigma}) + (2X_{2k_F, \sigma\sigma})^2 2X_{4k_F, \sigma-\sigma} \right\} \int dx A_{p\sigma}^2 A_{p-\sigma}^2 \\ + \frac{3}{8t^2} \sum_{p, \sigma} 2X_{2k_F, \sigma\sigma} (2X_{2k_F, \sigma-\sigma})^2 \int dx A_{p\sigma}^2 A_{p-\sigma}^2, \quad (\text{B}\cdot 8)$$

$$\mathcal{H}_{1/4}^a = \frac{1}{4t^2} \sum_{p, \sigma} \left\{ 2(2X_{2k_F, \sigma-\sigma})(2X_{2k_F, \sigma\sigma})(2X_{4k_F, \sigma\sigma} + 2X_{4k_F, \sigma-\sigma}) \right\} \int dx A_{p\sigma}^3 A_{p-\sigma} \\ + \frac{1}{8t^2} \sum_{p, \sigma} \left\{ 6X_{2k_F, \sigma-\sigma} (2X_{2k_F, \sigma\sigma})^2 + (2X_{2k_F, \sigma-\sigma})^3 \right\} \int dx A_{p\sigma}^3 A_{p-\sigma}, \quad (\text{B}\cdot 9)$$

$$\mathcal{H}_{1/4}^b = \frac{1}{4t^2} \sum_{p, \sigma} \left\{ (2X_{2k_F, \sigma\sigma})^2 (2X_{4k_F, \sigma\sigma}) + \frac{1}{2} (2X_{2k_F, \sigma\sigma})^3 \right\} \int dx A_{p\sigma}^4. \quad (\text{B}\cdot 10)$$

In the bosonized form, eqs. (B·8), (B·9) and (B·10) are proportional to $\int dx \cos 4\theta_\rho$, $\int dx \cos 4\theta_\rho \cos 2\theta_\sigma$ and $\int dx \cos 4\theta_\rho \cos 4\theta_\sigma$, respectively, and the scaling dimension of the respective term is given by $2 - 8K_\rho$, $2 - 8K_\rho - 2K_\sigma$ and $2 - 8K_\rho - 8K_\sigma$. Therefore eq. (B·8) has the largest scaling dimension. By substituting $2X_{2k_F, \sigma\sigma'} = Ua\delta_{\sigma, -\sigma'} - 2V_2a$ and $2X_{4k_F, \sigma\sigma'} = Ua\delta_{\sigma, -\sigma'} - 2V_1a + 2V_2a$ into eq. (B·8), one obtains eqs. (20a) and (20b). We note that the coupling constant of the Hamiltonian (B·9) is proportional to $2X_{2k_F, \sigma-\sigma} = Ua - 2V_2a$. Equation (B·10) becomes important for $K_\sigma < 1/4$ in the insulating state. However, the term, $\cos 2\theta_\sigma$ is already relevant for $K_\sigma < 1$, *i.e.*, $U < 2V_2$. Then we can safely neglect $\mathcal{H}_{1/4}^b$.

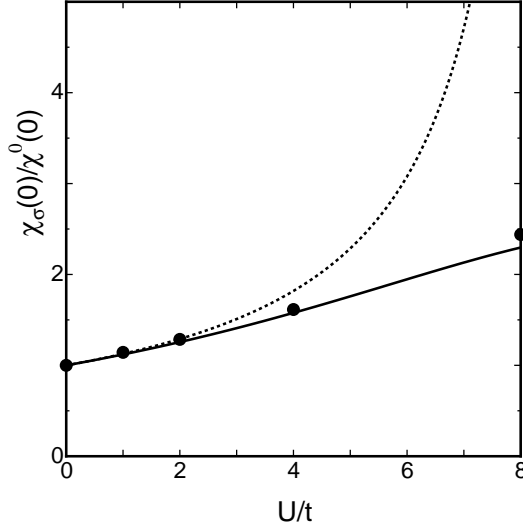


Fig. 8. Spin susceptibility of Hubbard model at $T = 0$ as a function of U/t , where $\chi^0(0)$ is the susceptibility in the absence of the interaction. The solid (dotted) curve expresses the spin susceptibility with (without) the virtual process to the upper band shown in Fig. 2. The solid circle is derived from the exact solution in ref. 24.

Appendix C: Spin Susceptibility at $T = 0$ for Hubbard Model with $U > 0$

In case of $V_1 = V_2 = 0$, $U > 0$ and $T = 0$, the spin susceptibility, eqs. (34) and (35), normalized by $\chi^0(0)$ reduces to,

$$\frac{\chi_\sigma(0)}{\chi^0(0)} = \frac{1}{1 - \frac{Ua}{2\pi v_F}(1 - UD_2)}. \quad (\text{C}\cdot 1)$$

We note that the D_2 -term originates from the virtual process to the upper band, which is not taken account in ref. 21. In Fig. 8, we show $\chi_\sigma(0)/\chi^0(0)$ with and without the virtual processes by solid curve and dotted curve, respectively, which are compared with the exact one (closed circle).²⁴⁾ As seen in Fig. 8, the spin susceptibility with the virtual processes is very close to the exact solution compared to that without the processes. It turns out that the virtual processes are necessary for quantitative estimation of the spin degree of freedom.

-
- [1] For review, see, D. Jérôme and H.J. Schulz: *Adv. Phys.* **31** (1982) 299, T. Ishiguro, K. Yamaji and G. Saito: *Organic Superconductors* (Springer-Verlag, Berlin, 1998).
 - [2] J. P. Pouget and S. Ravy: *J. Phys. I France* **6** (1996) 1501, *Synth. Met.* **85** (1997) 1532.
 - [3] K. Hiraki and K. Kanoda: *Phys. Rev. Lett.* **80** (1998) 4737, K. Kanoda, K. Miyagawa, A. Kawamoto and K. Hiraki: *J. Phys. IV France* **9** (1999) Pr10-353.
 - [4] S. Kagoshima, Y. Saso, M. Maesato, R. Kondo and T. Hasegawa: *Solid State Commun.* **110** (1999) 479.
 - [5] Y. Nogami, K. Oshima, K. Hiraki and K. Kanoda: *J. Phys. IV France* **9** (1999) Pr10-357.

- [6] K. Hiraki and K. Kanoda: Phys. Rev. B **54** (1996) R17276
- [7] F. Mila and X. Zotos: Europhys. Lett. **24** (1993) 133.
- [8] K. Penc and F. Mila: Phys. Rev. B **49** (1994) 9670.
- [9] K. Sano and Y. Ōno: J. Phys. Soc. Jpn. **63** (1994) 1250.
- [10] M. Nakamura, A. Kitazawa and K. Nomura: Phys. Rev. B **60** (1999) 7850.
- [11] H. Seo and H. Fukuyama: J. Phys. Soc. Jpn. **66** (1997) 1249.
- [12] Y. Suzumura: J. Phys. Soc. Jpn. **66** (1997) 3244.
- [13] N. Kobayashi, M. Ogata and K. Yonemitsu: J. Phys. Soc. Jpn. **67** (1998) 1098.
- [14] Y. Tomio and Y. Suzumura: J. Phys. Soc. Jpn. **69** (2000) 796.
- [15] M. Tsuchiizu, H. Yoshioka and Y. Suzumura: Physica B **284-288** (2000) 1547.
- [16] H. Yoshioka, M. Tsuchiizu and Y. Suzumura: J. Phys. Soc. Jpn. **69** (2000) 651.
- [17] The work has been partly reported in proceeding of CREST international workshop, *Pseudo Gap, Spin Gap, and Anomalous Metals*, H. Yoshioka, M. Tsuchiizu and Y. Suzumura, to be published in J. Phys. Chem. Solids.
- [18] T. Giamarchi and H. J. Schulz: J. Phys. France **49** (1988) 819, M. Tsuchiizu, H. Yoshioka and Y. Suzumura: Prog. Theor. Phys. **98** (1997) 1045.
- [19] T. Giamarchi and H. J. Schulz: Phys. Rev. B **39** (1989) 4620.
- [20] Note that the factor $G_{1/4}(l)$ in the exponential of the correlation function $\langle \cos 2\theta_\rho(x) \cos 2\theta_\rho(0) \rangle$ and $\langle \sin 2\theta_\rho(x) \sin 2\theta_\rho(0) \rangle$ comes from the non-linear term $\cos 4\theta_\rho$. On the hand, the factor does not appear in $\langle \cos \theta_\rho(x) \cos \theta_\rho(0) \rangle$ and $\langle \sin \theta_\rho(x) \sin \theta_\rho(0) \rangle$.
- [21] H. Néglise, C. Bourbonnais, H. Touchette, Y. M. Vilk and A. -M. S. Tremblay: Eur. Phys. J. B **12** (1999) 351.
- [22] T. B. Bahder and F. Woynarovich: Phys. Rev. B **33** (1986) 2114.
- [23] A. Luther: Phys. Rev. B **15** (1977) 403.
- [24] H. Shiba: Phys. Rev. B **6** (1972) 930.
- [25] J. W. Cannon and E. Fradkin: Phys. Rev. B **41** (1990) 9435.
- [26] J. Voit: Phys. Rev. B **45** (1992) 4027.
- [27] M. Nakamura: J. Phys. Soc. Jpn. **68** (1999) 3123, Phys. Rev. B **61** (2000) 16377.
- [28] M. Maesato, Y. Kaga, R. Kondo and S. Kagoshima: Rev. Sci. Instrum. **71** (2000) 176.